

FAN CASING CONTOURING UNDER CONSIDERATION OF AEROACOUSTICS, MECHANICS, AEROELASTICITY AND WHOLE ENGINE PERFORMANCE

A.-L. Aulich¹, T. Sauer², S. Iseni³, A. Moreau⁴, D. Peitsch², R. Mailach³, D. Micallef³, L. Enghardt⁴, E. Nicke¹

¹Deutsches Zentrum für Luft und Raumfahrt (DLR), Cologne, Germany; ²Technische Universität Berlin (TUB), Berlin, Germany; ³Ruhr-Universität Bochum (RUB), Bochum, Germany; ⁴Deutsches Zentrum für Luft und Raumfahrt (DLR), Berlin, Germany

Abstract

Aircraft propulsion will continue to rely on gas turbine technology for the next decades to come. Thus, to achieve environmental agreements, ensure engine safety and retain economic competitiveness, ongoing development with a multidisciplinary design approach is indispensable.

In the present study the multi criteria analysis of the fan, a decisive component in modern aero engines, is examined. In particular the interaction of the fan blades with the fan casing is analyzed and an appropriate design approach including automatic optimization is used.

As one part of the disciplines conjunction an automated aeroacoustic approach is realized. The aerodynamic and acoustic fitness functions and constraints are based on Reynolds-Averaged Navier-Stokes (RANS) simulations of the fan stage. A fast analytical prediction tool for fan noise, PropNoise, which has been under development since recent years and already validated on several test cases, is used.

Preliminary studies have shown that the flow in the rotor tip region is a major contributor to the broadband noise emission. Based on this, the optimization process focuses on the variation of the casing contour around the fan blades. The impact of the modified flow field in the rotor tip region concerning the aeroelastic behavior is also investigated. As aeroelastic evaluation requires a high level of know-how and is very time consuming, it is linked to the optimization process chain by a discrete evaluation of selected members. This allows a simultaneous adjustment of the design in case of aeroelastic issues.

Furthermore, the impact of the fan modifications regarding the overall engine performance is evaluated. Off-design cycle calculations allow incorporating such detailed studies in a global engine optimization.

1. INTRODUCTION

In this project, new casing contours around the rotor are investigated regarding the aerodynamic, acoustic and aeroelastic behaviors as well as the whole engine performance.

In the past, the acoustic design was concentrated on a preliminary definition of the main parameters responsible for the acoustic footprint of the fan (e.g. blade tip speed, blade counts of the rotor and the outlet guide vanes). The acoustic prediction was until now not included in the optimization process. In that project, the analytical prediction tool for fan noise, PropNoise, is implemented in the automated optimization.

In this work, the casing contour is to be optimized. A small number of parameters (8 points on the casing contour of the fan tip area) is used to address primary the acoustic fitness function and its relation with the aerodynamic performance. Then, for a few optimized members, the flutter prediction and the whole engine performance are evaluated.

2. NOMENCLATURE

CFD Computational Fluid Dynamic
DLR Deutsches Zentrum für Luft- und Raumfahrt (German Aerospace Center)

F Fitness Function
FEM Finite Element Method
FPR Fan Pressure Ratio
FSI Fluid-Structure-Interaction
HPC High Pressure Compressor
IAE International Aero Engines
IBPA Inter-Blade Phase Angle
ICM Influence Coefficient Method
ISA International Standard Atmosphere
ND Nodal Diameter
OP Operating Point
OPR Overall Pressure Ratio
RANS Reynolds-Averaged Navier-Stokes
SA Spalart-Allmaras
SFC Specific Fuel Consumption
SM Surge Margin
TET Turbine Entry Temperature
TRACE DLR, tool "Turbomachinery Research and Computational Environment
Travelling Wave Mode
DLR tool, "Trace To PropNoise"
UFFA Universal Fan Facility for Acoustics

C_w Influence coefficient
 E_{kin} Kinetic energy
 FN Net thrust
 N_{LP} Low pressure shaft speed

W_{CFD}	Aerodynamic work
Λ	Logarithmic decrement
σ	Inter-blade phase angle
q	Maximum vibration amplitude
η_{is}	Isentropic efficiency
μ	Bypass ratio

3. AUTOMATED AEROACOUSTIC OPTIMIZATION

3.1. Simulation Setup

The CFD model of the optimization configuration consists of the UFFA-Fan stage of the AneCom Aerotest GmbH.

The aerodynamic process chain consists of the following steps:

- Casing contouring generation: the casing contour is generated with the DLR in-house tool *gta*. The rotor height and tip contour are then automatically adapted to the new casing contour with a constant gap.
- 3-D CFD mesh generation: a structured multi-block mesh is generated with the DLR in-house tool *PyMesh*. The stage mesh has about 2.6 million cells. Wall functions are used as wall treatment on the end walls and on the OGV. On the rotor blade walls is a low Reynolds mesh used ($y^+ < 2.5$). The mesh radial resolution consists of 81 nodes in the rotor and 15 nodes in the tip clearance. The OGV is radially resolved with 59 layers.
- 3-D CFD simulations: the 3-D CFD simulations are performed with the Reynolds-averaged Navier-Stokes DLR in-house solver *TRACE* [1, 2] in the selected operating points.
- Post-processing: the Post-processing is performed with the in-house post-processing tool *Post*.

This is followed by the acoustic process steps. The here used approach follows the so called RANS-informed PropNoise (right side on FIGURE 1)

- T2P: is a post-processing tool that extracts the flow and geometry data from the 3-D CFD simulations and processes them to generate the input required by the acoustic models of PropNoise [3] (see FIGURE 1).
- PropNoise: is a fan noise prediction tool based on analytical models [4, 5]. It is fast, robust, and can handle different fan configurations (open or ducted, single- or counter-rotating). Tonal and broadband noise components can also be calculated simultaneously. In the present study the focus is put on the interaction between the rotor outflow (including the wakes and the tip vortex) with the stator vanes.

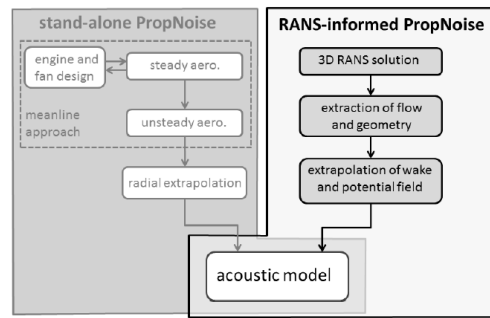


FIGURE 1. Process of the noise prediction

3.2. Free Variables

The optimization was performed with 8 free geometric parameters on the casing contour of the fan tip area (see FIGURE 2). The positions of these 8 points could only vary in the radial direction (± 5 mm) independently. The tip gap is kept constant, i.e. the rotor height is adapted to the new casing contour.

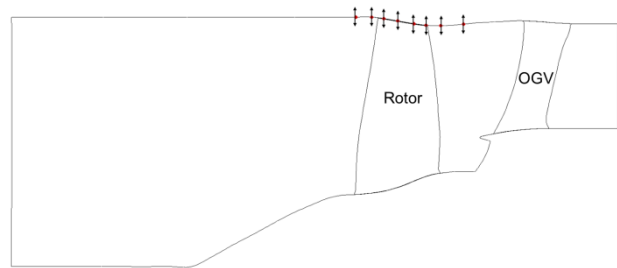


FIGURE 2. Calculation domain with the free parameters on the casing contour

3.3. Optimization Process

The flowchart in FIGURE 3 shows the basic structure of the parallelized multi-objective evolutionary algorithm *AutoOpti* [6, 7], developed at the Institute of Propulsion Technology of the DLR.

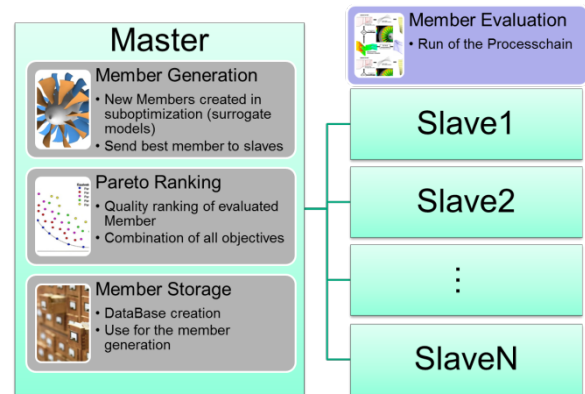


FIGURE 3. Flowchart of the optimization

3.4. Optimization Strategy

The goal of the optimization is to learn how the rotor exit flow – mainly in the outer part of the channel - could be optimal under acoustic considerations. Furthermore, the rotor isentropic efficiency at the design point, defined as the point with the maximum efficiency on the 100% speed line, has to be at least as good as the one of the initial

geometry. Finally, the stability margin of the fan has to be maintained.

Three operating points are considered:

- The aerodynamic design point (OP0) on the 100% speed line fixed at 124000 Pa pressure at the exit of the bypass. The exit pressure value comes from the initial member.
- The near surge line point (OP1) on the 100 % speed line. An increase of 3.2% of the OP0 exit pressure is set for the near surge line point OP1. This point is defined to secure as much stall margin as for the initial geometry.
- The near surge line point (OP2) on the 60% speed line fixed at 107000 Pa pressure at the exit of the bypass. As for OP0, the exit pressure value comes from the initial member. This point corresponds approximately to the approach flight condition, which is an operating point relevant for acoustic certification. As the rotor incidence is higher by 5° at this point compared to OP0, the rotor blades are relatively strongly loaded at approach. This has some implications during the optimization process, as discussed in the next section.

Two fitness functions are defined:

- F1 = maximize the rotor isentropic efficiency at OP0
- F2 = minimize the broad band noise at OP2

Two aerodynamic constraints are also defined:

- Criteria for power output: the fan total pressure ratio at OP0 must be comprised between: $1.49 < FPR(OP0) < 1.52$
- Criterion for stability margin: $FPR(OP1)/FPR(OP0) > 1.004$ the speed line must be at least as steep as for the initial geometry one.

3.5. Results of the Optimization

The optimization was stopped after 296 successfully evaluated members. The moderate number of free variables and the use of surrogate models enabled a fast converging optimization process.

It must be pointed out that, for a reason of confidentiality, only a delta isentropic efficiency ($\eta_{is}(Member) - \eta_{is}(Initial Member \text{ at } OP0)$) is presented in this paper.

FIGURE 4 shows the database of the optimization in the two-dimensional space defined by the fitness functions. The red scatter points represent the database, the green points the members of the database which fulfilled all the constraints and the blue point represents the initial geometry. Three optimized members have been selected on the pareto-front: Member 415, Member 462 and Member 515. The tip contours of the initial geometry and the three selected optimized members are represented in FIGURE 5.

It could be observed on FIGURE 4 that a compromise must be found between high rotor isentropic efficiency at OP0 and low broadband noise levels at OP2. This result may be striking at first, as broadband noise correlates relatively well with turbulence production, losses and thus with aerodynamic efficiency. This is indeed the case if we

consider efficiency at OP2. However the rotor efficiencies at OP0 and OP2 do not correlate well with each other: as mentioned in a previous section, the OP2 point is characterized by a high incidence.

The performance maps of the rotor and the fan for the initial geometry and the three optimized members are shown in FIGURE 6. The mass flow has become lower for the 100%- as well as the 80%-speed line. Moreover, though the rotor isentropic efficiency is kept constant to the same level, no improvement is observed. Furthermore the fan isentropic efficiency for the 100%-speed line is significantly decreased.

FIGURE 7 shows the Mach number contour at about 95% relative mass flow rate (near the casing) for the initial geometry and the three optimized members. It could be noticed that the stator is no more matching the incoming stream for the optimized members, it is completely detached. That explains the considerable decrease of the fan isentropic efficiency. Moreover, it is to suppose that, because of the unsuitable stator-circulation, no improvement of the rotor has been reached during the optimization. A stator optimization will probably enable to improve also the rotor. For this reason a second optimization is planned. In that optimization the casing contour around the rotor as well as the stator geometry will be optimized.

A more detailed analysis of the aerodynamic/acoustic optimization results are presented in [8].

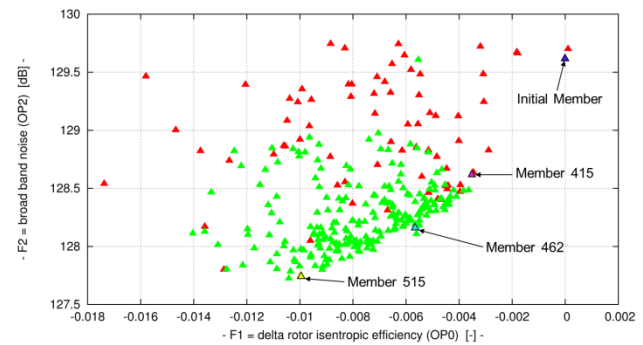


FIGURE 4. Database of the optimization – Broad band noise at OP2 vs. delta rotor isentropic efficiency at OP0

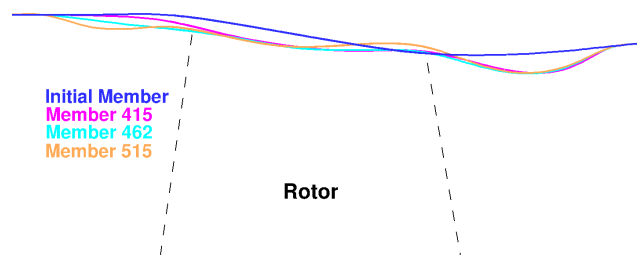


FIGURE 5. Casing contour of the initial geometry and the three selected optimized members

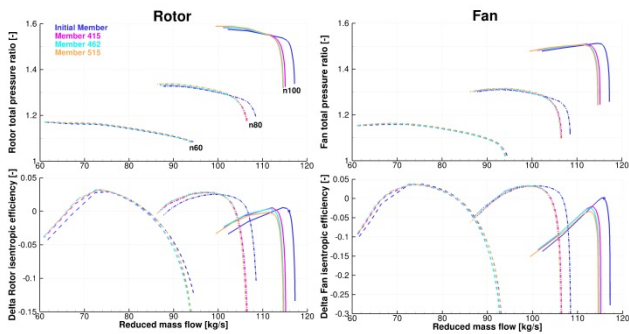


FIGURE 6. Performance maps of the rotor (left) and the fan stage (right) for the initial geometry and the three optimized members

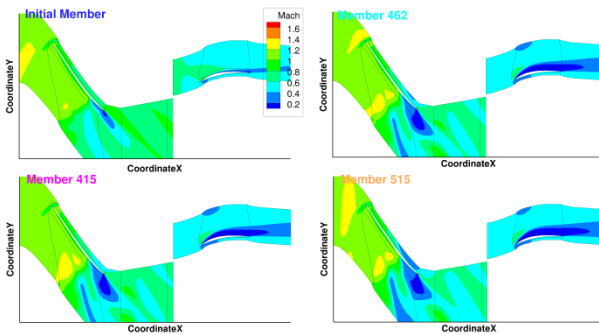


FIGURE 7. Mach number contours near the casing (95% relative mass flow rate) for the initial geometry and the optimized members at the design point OPO

4. FLUTTER PREDICTION

During the design process of jet engines the risk of flutter has to be considered. Flutter is a self-excited aeroelastic instability phenomena which can finally cause material fatigue, and in the worst case leads to blade failure within a very short period of time. The casing variation of the rotor tip has significant influence on aeroelastic behavior or the flutter stability. The workflow for accurate flutter stability analysis used for these investigations was published by [9] using the Traveling Wave Mode (TWM) formulation and is applied on the basic and optimized designs of the fan. Moreover, this workflow was extended by the Influence Coefficient Method (ICM) [10] to save computational time during the optimization process.

4.1. Overview of the Flutter Analyses Methods

To investigate the flutter risk behavior for all the fan rotor designs, one-way fluid-structure-interaction (FSI) simulations are performed, applying the so-called energy method introduced by Carta [11]. This assumption leads to a unidirectional coupled FSI between the structural and aerodynamic model. For this purpose, pre-stressed model analysis is performed using the FEM solver ANSYS (Mechanical) and a modified version (including FSI) of the 3-D flow solver TBLOCK for the unsteady CFD calculations. The flutter calculations are performed with a prescribed mode shape, constant frequency, as well as predetermined vibration amplitude.

The unsteady flow field with respect to the vibrating blades changes energy also referred to as aerodynamic work (W_{CFD})

$$(1) W_{CFD} = \int_t^{t+T} \left[\int_A -(\dot{\mathbf{x}} \cdot \mathbf{\bar{n}}p) dA \right] dt$$

with the blade during one period of oscillation. For that reason, an integration is carried out for fluid forces due to static pressure loads over the whole blade surface for the corresponding mode shape. The flutter stability is expressed by the logarithmic decrement (Λ) and is calculated by

$$(2) \Lambda = \frac{-W_{CFD}}{2E_{kin}}$$

considering the kinetic energy E_{kin} of the mode shape. A negative logarithmic decrement indicates a flutter risk and might lead to an amplified blade vibration and finally to blade failure.

Applying the ICM to a multi blade passage model, gives the stability curve over the nodal diameter (ND) or inter-blade phase angle (IBPA; σ) with only one CFD computation. In this case only the reference (middle) blade in a multi passage model is vibrating. Against it, all possible IBPA's has to be observed using the TWM method to get the entire stability curve. It is consequently very time-consuming.

4.2. Structural and Aerodynamic Model

The pre-stressed modal analyses are carried out for the first three eigenmodes including the blade fir-tree root and disk conjunction (FIGURE 8). The high mechanical loads at the contact areas of the fir-tree joint are investigated for different shaft speeds and friction coefficients using the commercial FEM solver ANSYS.

The nonlinear contact problem is solved using the Augmented-Lagrange-method. The maximal equivalent von Mises stresses at the blade root are within the safety margins corresponding to the yield strength. The qualitatively stress distribution is given in FIGURE 8. Because of the high rotational speeds and static pressure loads, the static deformations amount to maximal 2.34% (trailing edge at tip moving towards the suction side) with regard to the blade tip chord length. The natural frequency and corresponding mode shapes are calculated considering the change in the stiffness matrix. In this paper the first eigenmode was detailed investigated, due to the fact that the bending mode shows the lowest flutter stability.

TBLOCK is a block-structured RANS finite volume solver. The Spalart-Allmaras (SA) turbulence model was used for the subsequent studies. The flutter stability is predicted using both the ICM- and TWM-method, and then compared to each other. All TWM calculations are carried out using a phase-shifted boundary condition which was developed by He [12]. The aeroelastic behavior was primarily studied for all fan rotor designs at near stall conditions (OP1).

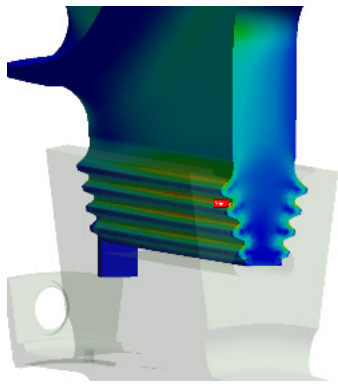


FIGURE 8. Fir-tree blade root von Mises stress distribution at design speed

4.3. Flutter Stability Analyses

The validation of the one-way flutter calculations were performed for the basis design with two different maximum amplitudes and two modes (see FIGURE 9) as well as a passage study with the ICM-method using 5 and 7 blade passages (see FIGURE 10). The amplitude variation (max. 0.5% and 1.0% of blade tip chord) in FIGURE 10 shows a typical linear or proportional relationship

$$(3) W_{CFD} \sim q^2$$

where the aerodynamic work is directly proportional to the square of the maximum vibration amplitude q for the corresponding nodal diameter. This justifies the linear system behavior assumption in a one-way calculation using the energy method. A good agreement between the ICM-method and the TWM stability curve exists for the 7 passage blade model. Both blade passage models (5 and 7 passages) predict and precisely determine the global minimum (ND=-1) of the local decrement. It should also be mentioned that the 7 blade passage model reflects the stability curve in a good manner and the computational costs can be reduced up to 70% in contrast to the TWM-method. The ICM-method was conducted for further optimization studies.

The imaginary part of the influence coefficients c_w is plotted for all designs and blade indices in the bar diagram FIGURE 11. The vibrating reference blade 0 affects his neighboring blades -1 and +1 for all designs, which results in a negative influence corresponding to the stability of the system. Every optimized design member reduces this fact in comparison to the basis design especially for blade -1. In contrast to that the other blades have a damping effect on the stability due to the interaction between fluid and blade structures.

The radial distributions of the logarithmic decrement for all the designs are plotted in FIGURE 12. A damping character could be seen starting from 40% blade span for the optimized designs corresponding to the flutter stability parameter Λ . According to the tip gap variation the most stable behavior shows the member 515.

In contrast to the other designs, a higher damping effect is reached for the member 515 at 70-80% blade span. This point could also be seen on the suction side near the tip region. Furthermore, for all the optimized members the destabilizing impact (highlighted red) of the basis in comparison to the other design on the suction side is minimized starting from 40% blade span.

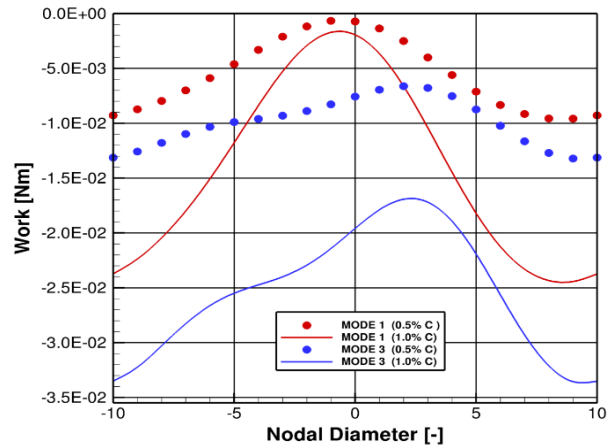


FIGURE 9. Energy Method Validation: Aerodynamic work vs nodal diameter for Mode 1 and 3 and two prescribed vibration amplitudes

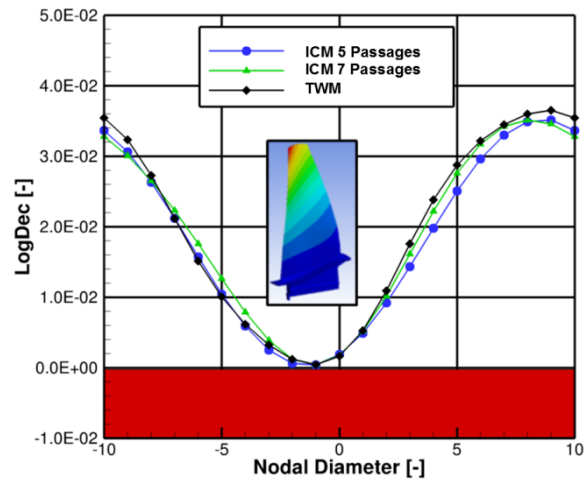


FIGURE 10. ICM-Method validation: Logarithmic decrement vs nodal diameter for Mode 1 using the TWM- and ICM formulation

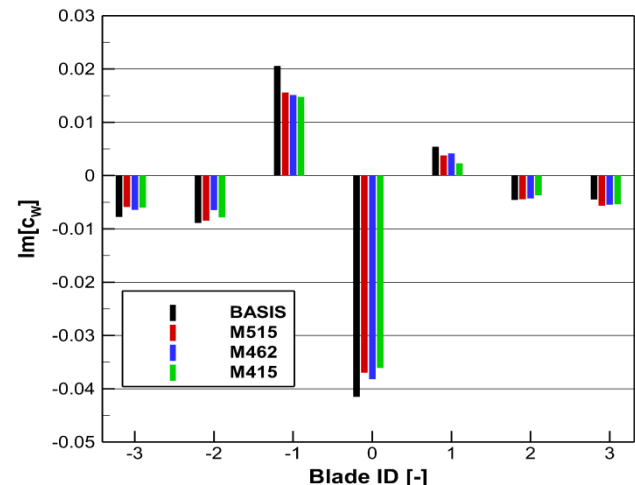


FIGURE 11. Imaginary part of the influence coefficients for all blades [-3, ..., 0, ..., +3] and optimized designs

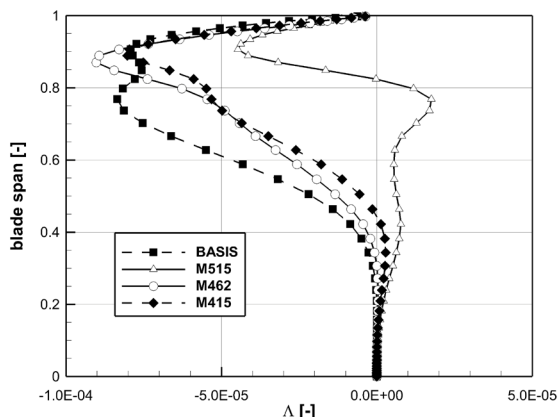


FIGURE 12. Radial distribution of logarithmic decrement averaged over the blade surface

5. WHOLE ENGINE PERFORMANCE

In order to evaluate the selected fan casing designs in a holistic context, their effects onto the whole engine needs to be assessed. Thus, cycle calculations are carried out by the gas turbine simulation environment *GTlab* developed by the German Aerospace Center.

5.1. Performance Model Setup

GTlab uses a synthesis architecture, so every component is represented by a single module. These modules are interconnected to allow the exchange of mass, energy and momentum of the fluid as well as the mechanical shaft power. In this one-dimensional modeling approach the gas properties are thermodynamically averaged over the components inflow and outflow cross sections. A numerical synthesis scheme controls the validity of the collective physical model in terms of mass, energy and momentum conservation [13].

The design of the applied synthesis model bases on a V2500-A5 engine, developed by International Aero Engines (IAE). Thus, a two shaft, booster charged aero engine as illustrated in FIGURE 13 is examined.

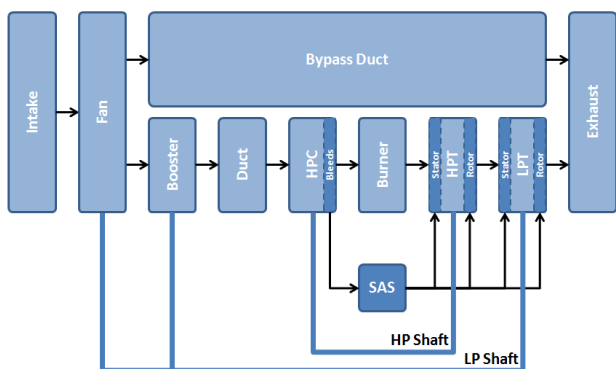


FIGURE 13. Architecture of examined synthesis model

The design point data of the synthesis model bases on take off information published by [14, 15]. The off-design behavior is derived by characteristics collected by Kurzke [16]. Thus, the fan casing modification can be evaluated in a flight operation context. The assessed operation points are defined in TAB 1. All points are referred to the

international standard atmosphere ISA and are controlled by the low pressure shaft speed N_{LP} .

	Altitude [m]	Mach number [-]	N_{LP} rate [%]
Take off	0	0	100
Cut back	500	0.35	80
Cruise	10668	0.8	92
Approach	120	0.2	60

TAB 1. Operating point conditions (ISA referred)

To compare the effects of the selected fan casing modifications only the fan module is adapted, i.e. the design point information as well as the off design characteristic of the reference configuration is replaced with the modified data. The other modules remain unaffected, except of an adjustment of the mass flow rate.

5.2. Effects on Engine Performance

The relative effect of the modified casings onto the specific fuel consumption *SFC* of the examined engine is presented in FIGURE 14. The reference equals the initial configuration. Looking at the take off and the cruise condition a distinct increase in *SFC* appears. This is explained with the reduction of the fan isentropic efficiency η_{is} in the upper power region as expressed in section 3.5. Furthermore, the modified configurations are characterized by a clear mass flow reduction in this power region, leading to an equivalent decrease in net thrust *FN* as expressed in FIGURE 15. Looking at the lower power region, i.e. cut back and approach, a *SFC* benefit is achieved. The primary contributors of this trend are the relative increase in η_{is} , the relative increase of the bypass ratio μ and the absence of a thrust reduction.

The relative effect onto the turbine entry temperature *TET* is shown in FIGURE 16. Again, the high power region, i.e. take off and cruise, differs from the low power region, represented by cut back and approach. The former is almost unaffected, because the η_{is} drop and the decrease of the overall pressure ratio *OPR* cancel each other out. The particular *OPR* reduction, as expressed in FIGURE 17, bases on the decreased fan pressure ratio *FPR*, as discussed in section 3.5. The latter is characterized by a high increase of the *TET*, resulting from the increase of the *OPR*.

So far the M515 configuration shows the most distinct performance changes, while the effect of the M415 configuration is most moderate. This is explained by the particular distribution within the noise-to-efficiency Pareto front as described in FIGURE 4 in which the M415 configuration is the closest to the reference.

The relative effects onto the surge margins *SM* of the particular compressor modules are shown in FIGURE 18 (fan), FIGURE 19 (booster) and FIGURE 18 (high pressure compressor, HPC). All modifications have a positive impact onto the fan and booster stability, while the fan is stabilized during high power operation and the booster during low power operation. Especially the M515 configuration leads to a significant stability benefit of the low pressure compressors. Due to the modified fan

characteristic, the particular operating points are shifted to a less loaded condition and the *SM* increases. Indeed, the HPC *SM* decreases during cut back and approach, because the operating points are moved to a higher load to compensate the less power of the low pressure compressors. The booster *SM* respectively HPC *SM* is not affected during take off, i.e. design point condition, because the particular pressure ratios are fixed.

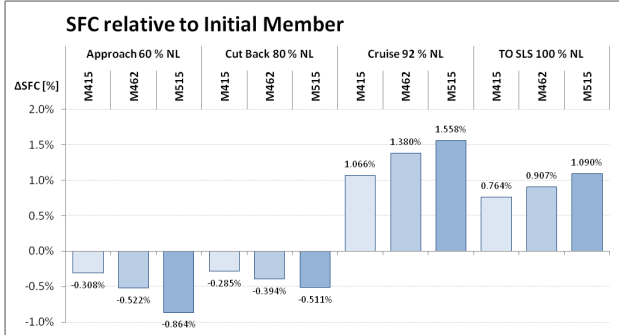


FIGURE 14. SFC effect of casing modifications relative to initial configuration

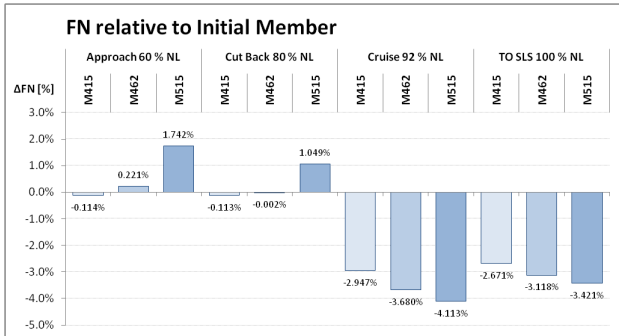


FIGURE 15. FN effect of casing modifications relative to initial configuration

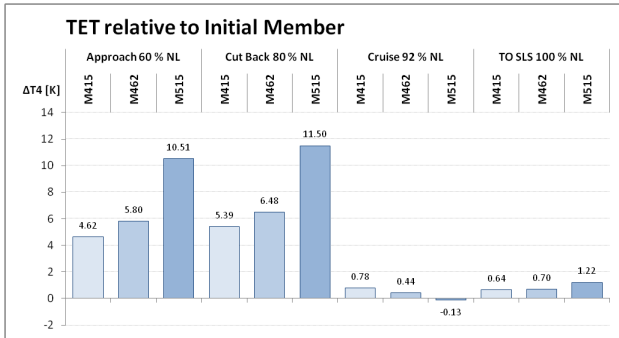


FIGURE 16. TET effect of casing modifications relative to initial configuration

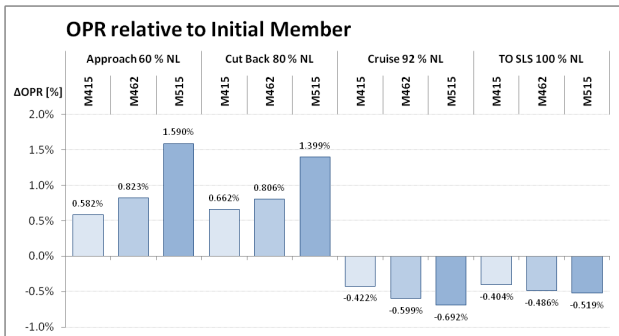


FIGURE 17. OPR effect of casing modifications relative to initial configuration

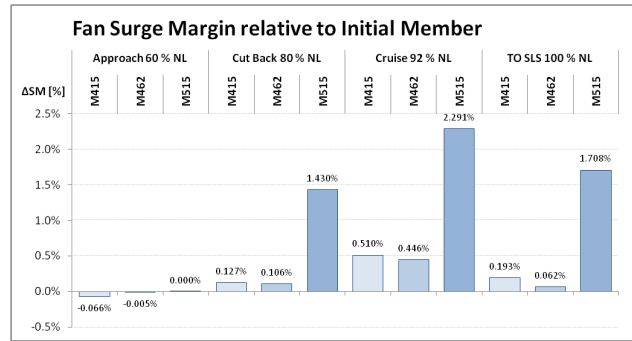


FIGURE 18. Fan SM effect of casing modifications relative to initial configuration

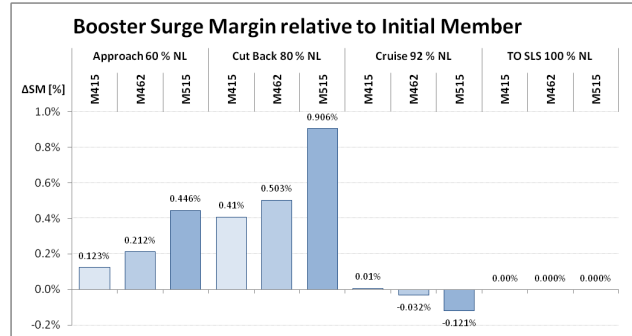


FIGURE 19. Booster SM effect of casing modifications relative to initial configuration

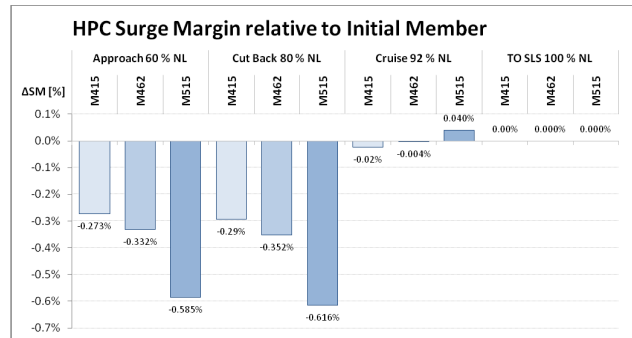


FIGURE 20. HPC SM effect of casing modifications relative to initial configuration

5.3. Engine Performance Assessment

Considering *SFC* during cruise condition, *FN* during cruise and take off condition and *TET* during cut back and approach condition all modifications are characterized by a distinct deficit relative to the initial configuration. Since member M415 shows the most moderate change, M415 is recommended in a noise-to-performance tradeoff. Considering the compressor stability effects, M415 shows the smallest increase in booster *SM* and clearly less improvement than M515 regarding the fan *SM*. However, M415 shows the least deficit in HPC *SM*, so M415 represents the most conservative choice.

Nevertheless, an enhancement of the parameter space applied for the optimization of the fan tip area is recommended to cancel the deficits regarding the main performance parameter.

The described process to assess the engine performance allows a simultaneous incorporation of the presented multidisciplinary optimization approach into a holistic framework.

6. CONCLUSION

The focus of this paper is a multidisciplinary study on a modification of the outer-casing contour of a high-bypass ratio fan.

First of all, an aeroacoustic automated optimization was performed to determine the best contour geometries. It is based on the integration into the design loop of a 3-D RANS solver (TRACE) and an analytical fan noise prediction model (PropNoise). The optimization revealed that a principle reduction in broadband noise of the rotor-stator interaction at approach flight conditions is possible with slight modifications of the casing contours (approx. 2 dB). However, this improvement is achieved at the expense of a loss in rotor efficiency by around one point in cruise flight conditions. Three optimized members on the pareto front have then been selected for detailed analysis of their aero-mechanical characteristics and their impact on global engine performance.

In order to accurately predict the aeroelastic behavior of the fan designs and successful adaption to the optimization process chain, flutter stability analysis was performed using Influence Coefficient Method. The fan casing modification also shows a strong influence on the flutter stability near the mid-span of the fan rotor. An improvement for mode 1 among all members is achieved by the casing variation near stall resulting into a higher aerodynamic damping.

Furthermore, to evaluate the selected fan casing designs, cycle calculations are carried out by *GTlab*. These calculations show that the performance of all three optimized members has decreased compared to the initial configuration. An extension of the parameter space is recommended to avoid these deficits regarding the main performance parameter.

The first major objective of the joint research project is fully fulfilled. Future fan concepts can be developed and/or assessed using the method of automatic optimization including aerodynamic, aeroacoustic, mechanical and FSI-models in the process chain. The results can be fed into an engine performance model for a direct assessment of the impact onto freely specified target functions like SFC, TET and so on.

The second objective, the development of specific casing treatments to reducing noise while maintaining the level of efficiency of the fan, is not reached yet. However, the presented results point into the right direction. In the next steps the drop of the mass flow rate (and therefore thrust) at cruise condition will be addressed by adapting the CFD-model. Additional free parameters will raise the potential to improve the efficiency of the whole fan stage. The rotor and especially the stator must be adapted to the new inlet flow conditions caused by the modified fan casing.

From now on, multidisciplinary "Design to Noise" will be a state-of-the-art approach, while there is still a lot to be developed.

7. ACKNOWLEDGMENTS

The authors are grateful to Henry Knobbe-Eschen from AneCom for providing the geometry and performance data of the UFFA-Fan. The authors would also like to acknowledge the financial support of the industrial partner Rolls-Royce Germany and the German Federal Ministry of Economic Affairs and Energy in the frame of the Aeronautical Research Program LuFo (project "FanTip", grant numbers 20E1304A, 20E1304B, and 20E1304C).

8. REFERENCES

- [1] Becker, K., Heitkamp, K. and Kügeler, E., 2010. "Recent progress in a hybrid-grid CFD solver for turbomachinery flows". ECCOMAS CFD 2010, Lisbon, Portugal
- [2] Kügeler, E., Weber, A., Nürnberger, D. and Engel, K., 2008. "Influence of blade fillets on the performance of a 15 stage gas turbine compressor". ASME Turbo-Expo 2008, Berlin, Germany GT2008-50748
- [3] Jaron, Moreau, Guérin, 2015. "Extrapolation of RANS flow data for improved analytical fan tone prediction", 21st AIAA/CEAS Aeroacoustics Conference, Dallas, AIAA-2015-2515
- [4] Moreau, Guérin, 2011. "Similarities of the free-field and in-duct formulations in rotor noise problems", 17th AIAA/CEAS Aeroacoustics Conference, Portland, AIAA-2011-2759
- [5] Moreau, Guérin, 2015. "The impact of low-speed fan design on noise: an exploratory study". ASME Turbo-Expo 2015, Montréal, Canada GT2015-43163 (2015).
- [6] M. Aulich, C. Voß, T. Raitor., 2014. "Optimization Strategies demonstrated on a Transonic Centrifugal Compressor". ISROMAC 15, 24.-28. Feb. 2014, Honolulu, USA.
- [7] C. Voß, M. Aulich, T. Raitor., 2014, "Metamodel Assisted Aeromechanical Optimization of a Transonic Centrifugal Compressor". ISROMAC 15, 24.-28. Feb. 2014, Honolulu, USA.
- [8] Moreau et al., "Optimization of casing contours in an aero-engine fan stage with emphasis on rotor-stator interaction noise", paper submitted to ISROMAC 2016 Conference.
- [9] Micallef, D., Witteck, D., Wiedermann, A. and Mailach, R., 2014: "An Efficient Workflow for Accurate Flutter Stability Analyses and Application to a State of the Art Compressor Rotor", ASME Paper No. GT2014-25646, ASME Turbo Expo, June 16-20, 2014, Düsseldorf, Germany.
- [10] May, M., Mauffrey, Y. and Sicot, F., 2011: "Numerical flutter analysis of turbomachinery bladings based on time-linearized, time-spectral and time-accurate simulations". In: Proceedings "IFASD 2011". IFASD 2011 - 15th International Forum on Aeroelasticity and Structural Dynamics
- [11] Carta, F., 1967. "Coupled Blade-Disk-Shroud Flutter Instabilities in Turbojet Engine Rotors". Journal of Engineering
- [12] He, L., 1990. "An Euler Solution for Unsteady Flows Around Oscillating Blades". ASME Journal of Turbomachinery, Vol. 112, pp. 714722.
- [13] Becker, R., Wolters, F., Nauroz, M. and Otten, T. "Development of a gas turbine performance code and its application to preliminary engine design". *Deutscher Luft- und Raumfahrtkongress 2011*, 241485, DLRK (Sep. 2011).
- [14] Gunston, B. (Ed.) *Jane's Aero-Engines*. Jane's Information Group, Coulsdon (2002), pp. 182-184.

- [15] Rick, H. *Gasturbinen und Flugantriebe*. Springer-Verlag, Berlin & Heidelberg (2013), pp. 715-738.
- [16] Kurzke, J. *Compressor and Turbine Maps for Gas Turbine Performance Computer Programs*. Self-published, Dachau (2004).